Bioresource Technology 291 (2019) 121919

Contents lists available at ScienceDirect

Bioresource Technology

journal homepage: www.elsevier.com/locate/biortech

Highly heterogeneous interior structure of biofilm wastewater for enhanced pollutant removals

Xianyang Li[a,b], Xiaodong Wang[a,b], Duu-Jong Lee[c,d,e,*], Wei-Mon Yan[f]

[a] Research Center of Engineering Thermophysics, North China Electric Power University, Beijing 102206, China
[b] School of Energy Power and Mechanical Engineering, North China Electric Power University, Beijing 102206, China
[c] Department of Chemical Engineering, National Taiwan University, Taipei 10617, Taiwan
[d] Department of Chemical Engineering, National Taiwan University of Science and Technology, National Taiwan University of Science and Technology, Taipei 10607, Taiwan
[e] College of Engineering, Tunghai University, Taichung 40704, Taiwan
[f] Department of Energy and Refrigerating Air-Conditioning Engineering, National Taipei University of Technology, Taipei 10608, Taiwan

GRAPHICAL ABSTRACT

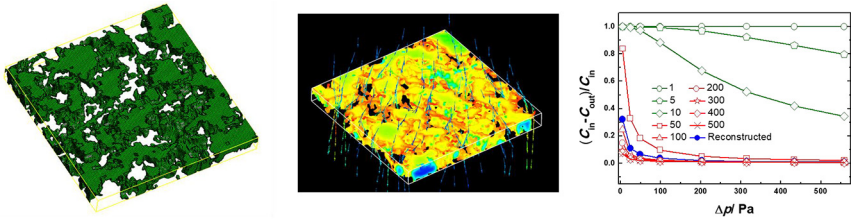

ARTICLE INFO

Keywords:
Interior structure
Multiple staining
Diffusion
Convection
Performance

ABSTRACT

Biofilm processes are widely used in wastewater treatment. The biofilm has highly heterogeneous interior structure, which can significantly affect the transport processes and the biological reactions over the biofilm. This study for the first time detailed the complicated velocity and concentration fields of substrate in a real biofilm structure. With a real biofilm interior being profiled and meshed to numerical solutions, the flow-through mode has significant distortion of inflow velocity fields and concentration distributions, which lead to enhanced biological reactions at regimes nearby major pores. Conversely, the crossflow mode depends weakly on the biofilm interior structure. The uniform biofilm model fails to describe the real biofilm processes. Future research needs based on real biofilm structures were discussed.

1. Introduction

Biological processes are cost-effective and environmentally friendly wastewater treatment units (Su et al., 2019; Gao et al., 2019). Compared with the suspended growth biological processes (Lee, 1994), the biofilm bioreactor can keep excess biomass in the reactor so the applied volumetric loading rates for pollutants can be increased (Guo et al., 2019; Peng et al., 2019). Wide range of biofilm reactors were applied in wastewater treatment, such as trickling filter, rotating disc contactor, submerged reactor, moving bed reactor, and others (Phuong et al., 2018; Meeta et al., 2019). The biofilm as the residential site of functional strains incorporating numerous intra-biofilm transport and reaction processes present the core to determine the performances of biofilm wastewater treatment processes (Gordon et al., 2019).

The biofilm has highly heterogeneous structure (Berk et al., 2012). Some studies commented that the heterogeneity of bioaggregates

：生物膜具有高度不均匀的结构

* Corresponding author at: Department of Chemical Engineering, National Taiwan University, Taipei 10617, Taiwan.

https://doi.org/10.1016/j.biortech.2019.121919
Received 26 June 2019; Received in revised form 24 July 2019; Accepted 25 July 2019
Available online 27 July 2019
0960-8524/

significantly affects the intra-biofilm diffusion rates of pollutants (Guiot et al., 2002; Chu and Lee, 2004). Conversely, others claimed that the fundamental constraints for biofilm processes were not affected by the structural heterogeneity (Steward, 2003). The advection and diffusion of individual cells determines the patterns of bacterial attachment and development in a matrix (Rossy et al., 2019). The biofilm models commonly assumed that the biofilm is a porous medium with constant porosity and permeability or with pore phases and matrix phase (Yen et al., 2002; Chang et al., 2019). The latter was assumed to be a constant porous medium (Landa-Marban et al., 2019). These assumptions simplified the analysis details, but also can lead to unrealistic prediction for practical processes (discussed later).

Chen et al. (2006) for the first time applied multiple staining technique to determine the three-dimensional distributions of four components of extracellular polymeric substances in a fouling layer on a membrane. These authors adopted simulations based on the reconstructed grids from the staining images, and noted that the initial fouling layer on membrane surface is very different in composition from those in the upper, surface layers. The multiple staining technique is an ideal probing tool to construct the detailed structures of a biofilm (Pan et al., 2016). Using the established grids, the transport processes in biofilm can be studied based on real structure probed by living biofilm (Yang et al., 2007).

It is unclear what is the niche the microorganisms would establish by making the biofilm a highly heterogeneous instead of a uniform interior (Kroukamp et al., 2019). To the authors' best knowledge, there is no previous research focusing on the substrate removal rates in the highly heterogeneous biofilm. This paper established the three-dimensional structural model based on real biofilm using the protocols by Adav et al. (2010), and then established the fluid flow and substrate concentration fields by solving the governing equations and boundary conditions. The strategy taken by the incorporated microorganisms for making the biofilm structure with enhanced substrate removal was discussed.

2. Establishment of the biofilm model

2.1. Biofilm cultivation

The waste-activated sludge collected from a local wastewater treatment plant which treated industrial wastewater with chemical oxygen demand over 15,000 mg/L was the seed sludge. The waste-activated sludge was ultrasonically dispersed for 3 min and was mixed with a cellulose acetate filter paper in a cultivation medium containing 250 mg/L yeast extract, 400 mg/L peptone, 4 mM NH_4Cl, 5 mM KH_2PO_4, 0.2 mM $CaCl_2$, 0.2 mM $MgSO_4$, 0.1 mM $FeSO_4$, and 500 mg/L glucose. The biofilm on the filter paper was developed in seven days of cultivation. The filter paper with the formed biofilm was rinsed with DI water and was placed in a pool containing the cultivation medium and was applied with a suction pressure of 0.5 atm for forcing the medium to flow through the filter. The COD was reduced based on biological activity of the biofilm. The biofilm was regarded mature and ready for further analysis.

2.2. Staining and imaging protocols

The image scanning and further processing protocols were modified from Adav et al. (2010). The fluorescein isothiocynate (FITC), SYTO 63 and labeled lectin Concanavalin A (Con A) purchased from Molecular Probes (Eugene, OR, USA) were reacted with amine-containing compounds, intracellular DNA, and alpha-mannopyranosyl and alpha-glucopyranosyl sugar residuals in the biofilm sample, respectively. The calcofluor white was purchased from Sigma-Aldrich (St. Louis, MO, USA) to react with beta-D-glucopyranose polysaccharides. The staining sequence was as follows: 20 μM SYTO 63 for 30 min, 10 g/L FITC for 60 min, 0.2 g/L Con A for 30 min, and 300 mg/L calcofluor white for 30 min, in between phosphate-buffered saline was used for rinsing. The stained biofilm was immediately scanned using Confocal laser scanning microscopy (TCS SP2 Confocal Spectral Miscoscope Imaging System, Leica, Wetzlar, Germany) with scanning area of $238 \times 238\ \mu m^2$ at 512×512 pixels in resolution, and scanning interval of 0.6 μm.

2.3. Mesh generation and computation

The images were processed by equalization, binarization, resampling, and then three-dimensional reconstruction with marching cubes and advancing-front algorithm to yield the discrete meshes for the studied biofilm. The so-produced meshes were established, named the reconstructed biofilm herein.

The meshes were established for the two regions, in the pore region and in the solid region. The governing equations for the fluid flow with the pollutant at concentration C were used for fluid flow and concentration fields in the pore region considering the equation of continuity, Navior-Stokes equation and mass conservation equation as follows:

Fluid phase:

$$\nabla \cdot \vec{V} = 0 \tag{1}$$

$$\rho_f (\vec{V} \cdot \nabla)\vec{V} = -\nabla p + \mu_f \nabla^2 \vec{V} \tag{2}$$

$$-\vec{V} \cdot \nabla c + D_f \nabla^2 c = 0 \tag{3}$$

Porous solid phase:

$$D_s \nabla^2 c + kc = 0 \tag{4}$$

A biofilm model with uniform structure and the same overall porosity and volume of the reconstructed model was applied as comparison basis. The diffusivity of the uniform model was estimated by Ergun equation as a function of porosity (ε) and constituting particle diameter (D_p) as follows:

$$\alpha = \frac{D_p^2}{150} \frac{\varepsilon^3}{(1-\varepsilon)^2} \tag{5}$$

The α values at $\varepsilon = 0.54$ are 4.96×10^{-15}, 1.24×10^{-13}, 4.96×10^{-13}, 1.24×10^{-11}, 4.96×10^{-11}, 1.98×10^{-10}, 4.47×10^{-10}, 7.94×10^{-10}, and $1.24 \times 10^{-9}\ m^2$ at D_p = 1, 5, 10, 50, 100, 200, 300, 400 and 500 μm, respectively. The governing equations for the Fluid phase are still Eqs. (1)–(3), while for the porous solid phase, the governing equations are

$$\rho_f (\vec{V} \cdot \nabla)\vec{V} = -\nabla p + \mu_f \nabla^2 \vec{V} - \left(\frac{\mu_f}{\alpha}\vec{V} + C_2 \frac{1}{2}\rho |\vec{V}| \vec{V} \right) \tag{6}$$

$$-\varepsilon \vec{V} \cdot \nabla c + D_{eff} \nabla^2 c + (1-\varepsilon) kc = 0 \tag{7}$$

$$D_{eff} = \varepsilon D_f + (1-\varepsilon) D_s \tag{8}$$

The boundary conditions are as follows:

Inlet: $u = v = 0$, $w = w_{in}$, $c = c_{in}$;
Outlet: $p = p_{out}$;
Fluid-solid interface: $v = u = w = 0$, $c_f = c_s$, $D_f \nabla c_f = D_s \nabla c_s$;
Other external surfaces: $\partial \vec{V}/\partial n = 0$, $\partial c/\partial n = 0$;

In simulation, two flow modes were studied: crossflow and flow-through modes (Fig. 1). For the former, a uniform water flow with pollutant concentration C_{in} was flowing from left to right over a biofilm. For the latter, a uniform water flow normal to the biofilm with pollutant of concentration C_{in}. As the water approaches the top surface of the biofilm layer, the flow pattern would be redistributed owing to the local solid structure. The pressure and concentration drops across the biofilm are numerically obtained. Numerical simulations were conducted using ICEM CFD 19.1 for mesh construction and Fluent 19.1 for equation

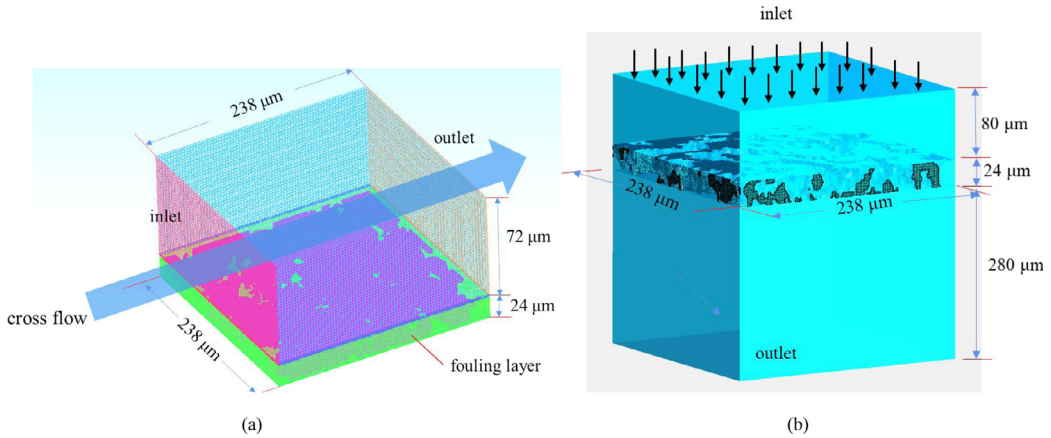

Fig. 1. The computation domain adopted in the present study. (a) Crossflow mode. (b) Flow-through mode. The size of biofilm layer is 238 μm × 238 μm × 24 μm.

solving with convergence criteria of 10^{-6}. The overall pollutant conversion of pollutant and fluid Reynolds number are defined as follows:

$$\eta = \frac{(c_{in} - c_{out})}{c_{in}} \tag{9}$$

$$Re = \frac{u_{in} D}{\nu} \tag{10}$$

where c_{in}, c_{out} are the inlet and outlet concentrations, respectively, u_{in} is inlet velocity, $D = 238$ μm, and ν is water kinetic viscosity. The interior diffusivities of solid phases were taken as 1.5×10^{-9} m^2/s if not otherwise mentioned. The fluid density was taken as kg/m^3, viscosity was 0.001003 kg/m-s. The average concentration of pollutant was calculated using mass-weight average, which is an average based on local mass flux and concentration. The average concentration based on surface area average was also adopted in the latter section for discussion.

3. Results and discussion

3.1. Crossflow mode

The velocity and concentration distributions along the centerline for the reconstructed biofilm and the uniform biofilm under crossflow mode with $Re = 4$ and $k = 250$ show a boundary-layer like profile, with certain circulations occurred for the reconstructed biofilm. However, the concentration profiles were only mildly distorted by the heterogeneous interiors of biofilm. The pressure drop and the η values for the reconstructed biofilm and the uniform biofilm at $k = 250$ and different crossflow rate demonstrated that: at low crossflow rate, the pressure drop is low but conversion is high (about 38%); at higher crossflow rate the conversion is low and shows insignificant difference of conversion for the two flow modes (Fig. 2). Restated, at the crossflow mode since most pollutant is transferred into the biofilm by molecular diffusion, the interior structure can only minimally impact the pollutant conversion rates. This finding correlates with the output by Steward (2003).

3.2. Flow-through mode

The three-dimensional velocity field and the concentration distributions for reconstructed biofilm under flow-through mode at 5, 10 and 20 μm from biofilm bottom showed that local velocities are significantly distorted from the normal flow direction owing to the obstacles of solid phase. The concentration varies significantly over the cross-sections of biofilm at different levels, while the ones at bottom layer do not necessarily higher than those at top layers. Certain circulation flows must exist inside the biofilm to bring the unreacted pollutant backward with the flowing stream so the complicated patterns

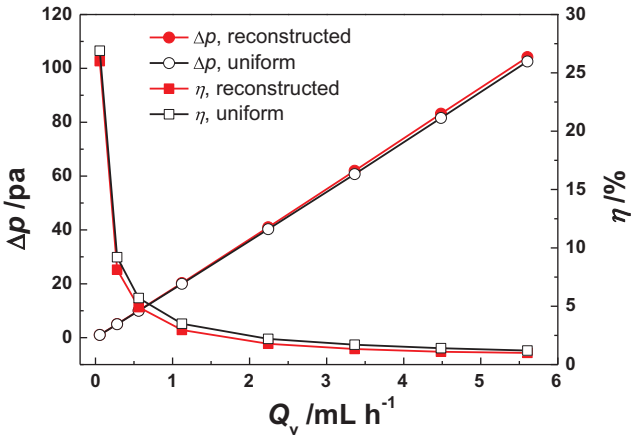

Fig. 2. Pressure drop and conversion of substrate for reconstructed and uniform biofilm models under crossflow mode. $Re = 4$ and $k = 250$. Porosity = 0.537 and permeability = 4.68×10^{-12} m^2.

can be observed.

Fig. 3 reveals the velocity and concentration profiles along the centerline for the reconstructed biofilm. The velocity through the major pores is much higher than those through minor pores (ret spots in Fig. 3a), and this high flow velocity leads to low concentration regimes inside the large solid clusters (Fig. 3b).

Fig. 4a shows the conversion of substrates from reconstructed biofilm at $Re = 1$ and with different k values. Although the k value has reached 2500, the conversion is still increased with k, suggesting that the reaction rate is one of the controlling steps of pollutant removal processes for this particular biofilm. At the same Re the influent pollutant quantity is the same, so the higher rate constant is beneficial to the substrate removal.

Fig. 4b shows the conversion of pollutant for reconstructed model as a function of pressure drop (blue circles). At low cross-biofilm pressure drop, the time of substrate reaction is long so the conversion is high. As cross-biofilm pressure drop is increased, the time of contact of pollutant and biomass, so the conversion, is reduced. The simulation results for uniform biofilm with different D_p are also shown in the figure for comparison. The conversion is high at small D_p since the flow rate is very low and contact time is very long. As D_p is increased, the flow rate is increased so the conversion is reduced. Among the simulation results shown in Fig. 5b, the uniform model with $D_p = 100$ μm best fits the reconstructed model than with other D_p.

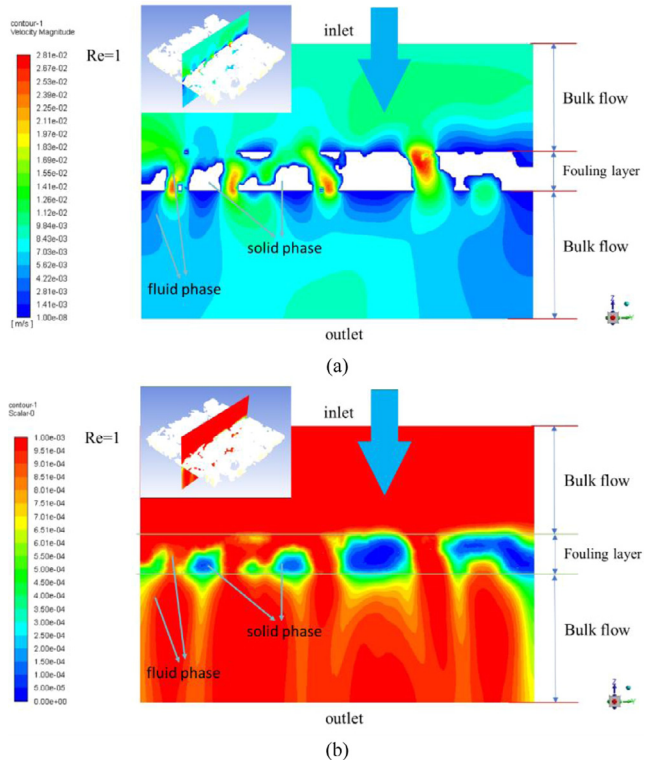

Fig. 3. Reconstructed biofilm under flow-through mode. $Re = 1$ and $k = 250$. (a) Velocity profiles; (b) concentration field.

3.3. Detailed biofilm processes

The biofilm processes were widely applied in applications but their detailed mechanisms are far from satisfactorily explores (Song et al., 2018). However, the common approach is to analyze the microbial community in the working biofilm (Tang et al., 2018; Ren et al., 2018; Arij et al., 2018) but to comprehend the local environments for the functional strains, therefore, cannot predict correct how the biofilm would perform in wastewater treatment. The present study reveals the drawbacks of uniform biofilm model which cannot catch the real transport processes and reactions inside the complicated structural networks of biofilm. At flow-through mode operation, this drawback is insignificant since the flow is in laminar regime and the main mechanisms for pollutant transport is molecular diffusion. Conversely, under crossflow mode all detailed structure with permeable pathway for water stream could contribute to the biofilm processes, the incapability of uniform biofilm model is obvious.

As Fig. 4b shows, the conversion of pollutant (η) is declined with pressure drop, which seems suggests that the microorganisms would fail to efficiently access nutrient at high flow-through velocity. One intuition is microorganisms in biofilm preferred a structure leading to high η. The total pollutant removal rate, in the unit of C_{in} can be calculated as product of influent mass flow rate times C_{in} and conversion. The ratios of total removal rates at Δp = 4.8, 24.2, 48.5, 98.1, 203, 315, 433, 558 Pa are 1:1.71:2.04:2.37:2.69:2.88:3.00:3.10. Restated, the microorganisms in biofilm can consume more pollutant at high influent velocity, even though the average conversion is reduced. The simulation results for uniform biofilm with D_p = 1 μm (the cells are of size of around 1 μm) have almost no flow owing to extremely high flow resistance in the biofilm, so although the conversion is unity the removal quantity of pollutant is effectively null. With large D_p, the conversion is declined with pressure drop imposed to the biofilm, while the flow rate is also increased. However, the best-fit is with D_p = 100 μm, which is four time to the total thickness of the studied reconstructed model

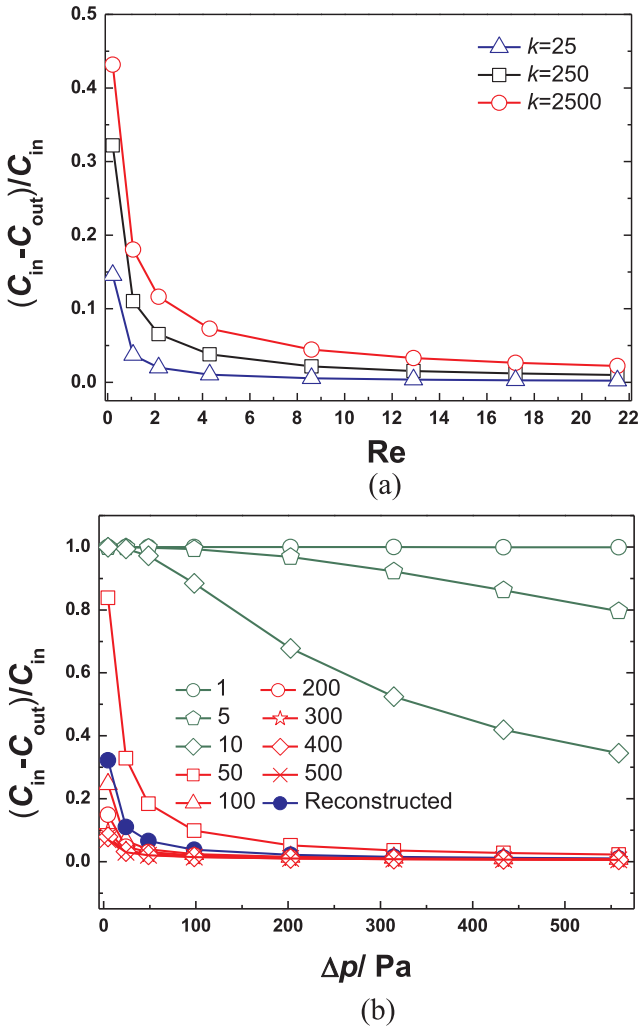

Fig. 4. Conversion of substrate by biofilm at flow-through mode. Reconstructed model. (a) Effects of Reynolds number at different k values; (b) Effects of pressure drop. Porosity = 0.537. k = 250. Solid circles: reconstructed model. Open symbols: uniform model with number for values of D_p.

(24 μm), demonstrating the incapability of uniform model to describe the detailed flow field and local reaction rates over the biofilm.

Fig. 5 shows the mean concentration along the flow direction based on area or on mass flux average. The area-average concentration would rebound across the biofilm, suggesting that some meshes of the bottom surface have higher concentrations than the ones at the upper layers of biofilm. Conversely, the mass flux average concentration shows monotonically decrease along the flow direction, a physically acceptable scenario. Microorganisms make major pores to allow high mass flow through them, though the local conversion of pollutant is reduced, the total removal quantity is increased. The high flow-through velocity enhances liquid-solid mass transfer rate, so accelerate local pollutant removal rates. The total quantity of pollutant consumed per unit time by the microorganisms around major pores is thereby increased. The minor pores allow low flow-through velocity, prolong the contact time so increase the conversion rate of pollutant. But since the velocity is low, the total mass flux of pollutant being removed through minor pores is reduced. The microorganisms near the minor pores have no competitive advantages to those near the major pores. This is the niche the biofilm with highly heterogeneous structure gives the constituent microorganisms competitive edge over the uniform biofilm.

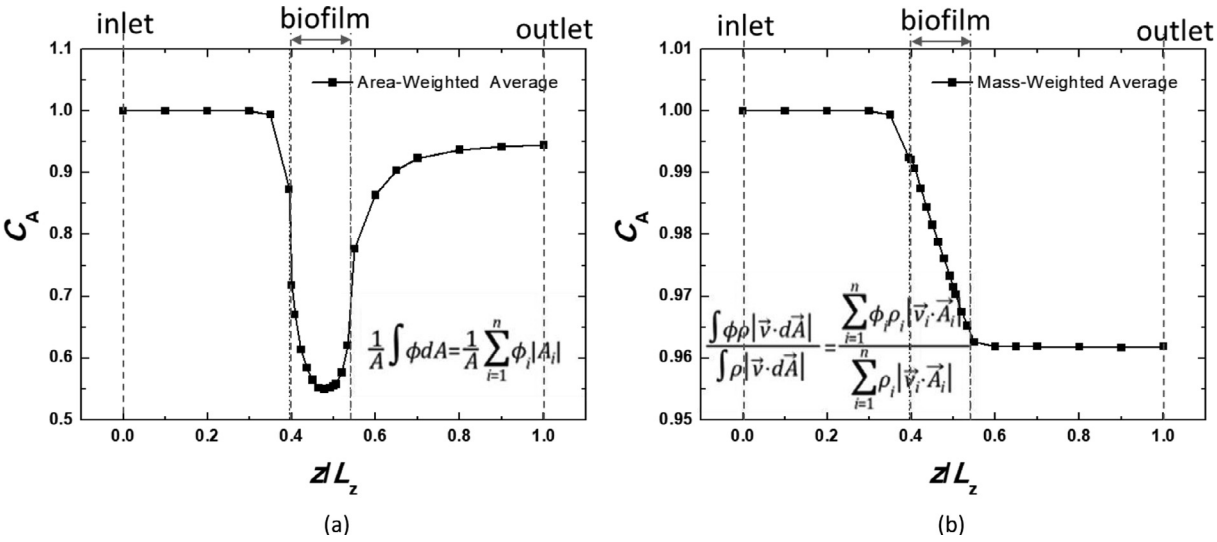

Fig. 5. Average concentration along flow direction. Crossflow mode. $Re = 1$, $k = 250$. (a) Area average; (b) flow rate average. $Re = 1$, $k = 250$.

3.4. Perspective

The present study provides the first study on biofilm processes considering the fluid flow and concentration fields in a working biofilm. As the results show, the commonly adopted uniform biofilm model in literature would overestimate the process performance with the real process parameters, or underestimate the process parameters if the uniform layer assumption is adopted. Therefore, the mathematical model with enhanced precision on performance prediction should be developed based on real biofilm structure.

Additionally, the finding that the microorganisms prefer to stay around the large pores with enhanced the local interfacial mass flux of substrates provide guidance for design of supporting carrier with large pores for biofilm formation. Restated, at the same internal porosity the matrix with larger pores would generate biofilm of higher reaction efficiency of substrates. Also, the carriers with non-uniform shape can promote formation of heterogeneous biofilm surface. Researches on the carrier design and biofilm structure should be performed.

The model adopted is based on real biofilm structure and the governing equations are for general conservation of momentum and mass laws, therefore, the main assumptions adopted herein are the process parameters being taken into modeling. Since the model is general to biofilm processes, the parameters such as k, diffusivity, porosity should be refined to be used for modeling different biofilm processes. The conclusions obtained herein are based on a specific set of process parameters, but should be generally valid for different biofilm processes. Estimation of process parameters in complex biofilm matrix would be a challenge for precise description of biofilm processes in operation.

4. Conclusions

The pollutant removal by a biofilm with real, heterogeneous structure was for the first time numerically studied. The substrate removal rate is insignificantly affected by the interior structure when operating in crossflow mode. In flow-through mode, the reconstructed biofilm shows complicated fluid velocity and concentration distributions over the biofilm. Microorganisms residing near major pores in the biofilm has advantage to access additional substrates than the counterparts residing near the minor pores. The heterogeneous biofilm is proposed by providing competition niche to its constituent microorganisms with excess substrate with enhanced intra-pore fluid-solid mass transfer rate to those in uniform biofilm.

Acknowledgments

This study was partially supported by the National Science Fund for Distinguished Young Scholars of China (No. 51525602).

Appendix A. Supplementary material

Supplementary data to this article can be found online at https://doi.org/10.1016/j.biortech.2019.121919.

References

Adav, S.S., Lin, J.C.T., Yang, Z., Whiteley, C.G., Lee, D.J., Peng, X.F., 2010. Sterological assessment of extracellular polymeric substances, exo-enzymes, and specific bacterial strains in bioaggregates using fluorescence experiments. Biotechnol. Adv. 28, 255–280.

Arij, Y., Fatihah, S., Rakmi, A.R., 2018. Performance of pilot scale anaerobic biofilm digester (ABD) for the treatment of leachate from a municipal waste transfer station. Bioresour. Technol. 260, 213–220.

Berk, V., Fong, J.C.N., Dempsey, G.T., Develioglu, O.N., Zhuang, X., Liphardt, J., Yildiz, F.H., Chu, S., 2012. Molecular architecture and assembly principles of *Vibrio cholera* biofilms. Science 337, 236–239.

Chang, Y.R., Lee, Y.J., Lee, D.J., 2019. Membrane fouling during water or wastewater treatments: Current research updated. J. Taiwan Inst. Chem. Eng. 94, 88–96.

Chen, M.Y., Lee, D.J., Yang, Z., Peng, X.F., 2006. Fluorescent staining for study of extracellular polymeric substances in membrane biofouling layers. Environ. Sci. Technol. 40, 6642–6646.

Chu, C.P., Lee, D.J., 2004. Multiscale structures of biological flocs. Chem. Eng. Sci. 59, 1875–1883.

Gao, J.F., Liu, X.H., Fan, X.Y., Dai, H.H., 2019. Effects of triclosan on performance, microbial community and antibiotic resistance genes during partial denitrification in a sequencing moving bed biofilm reactor. Bioresour. Technol. 281, 326–334.

Gordon, V., Bakhtiari, L., Kovach, K., 2019. From molecules to multispecies ecosystems: the role of structure in bacterial biofilms. Phys. Biol. 16, 041001.

Guiot, E., Georges, P., Brun, A., Fontaine-Aupart, M.P., Bellon-Fontaine, M.N., Briandet, R., 2002. Heterogeneity of diffusion inside microbial biofilms determined by fluorescence correlation spectroscopy under two-photon excitation. Photochem. Photobiol. 75, 570–578.

Guo, X., Li, B., Zhao, R., Zhang, J.Y., Lin, L., Zhang, G.J., Li, R.H., Liu, J., Li, P., Li, Y.Y., 2019. Performance and bacterial community of moving bed biofilm reactors with various biocarriers treating primary wastewater effluent with a low organic strength and low C/N ratio. Bioresour. Technol. 287, 121424.

Kroukamp, O., Bester, E., Wolfaardt, G.M., 2019. Biofilms: Besieged cities or thriving ports? In: In: Hurst, C. (Ed.), The Structure and Function of Aquatic Microbial Communities. Advances in Environmental Microbiology, vol. 7 Springer, Cham.

Landa-Marban, D., Liu, N., Pop, I.S., Kumar, K., Pettersson, P., Bodtker, G., Skauge, T., Rabu, F.A., 2019. A pore-scale model for permeable biofilm: Numerical simulations and laboratory experiments. Transport Porous Media 127, 643–660.

Lee, D.J., 1994. Floc structure and bound water-content in excess activated sludges. J. Taiwan Inst. Chem. Eng. 25, 201–207.

Meeta, R.A.A., Kannah, R.Y., Singhu, J., Ragavi, J., Kumar, G., Gunasekaran, M., Rajesh Banu, J., 2019. Trends and resource recovery in biological wastewater treatment system. Bioresour. Technol. Rep. 7, 100235.

Pan, M., Zhu, L., Chen, L., Qiu, Y.P., Wang, J., 2016. Detection techniques for extracellular polymeric substances in biofilms; A review. BioResources 11, 8092–8115.
Peng, C., Gao, Y., Fan, X., Peng, P.C., Huang, H., Zhang, X.X., Ren, H.Q., 2019. Enhanced biofilm formation and denitrification in biofilters for advanced nitrogen removal by rhamnolipid addition. Bioresour. Technol. 287, 121–387.
Phuong, N.T.T., Tien, T.T., Hoa, P.T.T., Nam, T.V., Luu, T.L., 2018. Treatment of cake shop wastewater by pilot-scale submerged membrane bioreactor (SMBR). Bioresour. Technol. Rep. 4, 101–105.
Ren, L.F., Lv, L., Kang, Q., Gao, B.Y., Ni, S.Q., Chen, Y.H., Xu, S.P., 2018. Microbial dynamics of biofilm and suspended flocs in anammox membrane bioreactor: The effect of non-woven fabric membrane. Bioresour. Technol. 247, 259–266.
Rossy, T., Nadell, C.D., Persat, A., 2019. Cellular advective-diffusion drives the emergence of bacterial surface colonization patterns and heterogeneity. Nat. Comm. 10, 2471.
Song, T.W., Li, S.S., Ding, W.D., Li, H.S., Bao, M.T., Li, Y., 2018. Biodegradation of hydrolyzed polyacrylamide by the combined expanded granular sludge bed reactor-aerobic biofilm reactor biosystem and key microorganisms involved in this bioprocess. Bioresour. Technol. 263, 153–162.
Steward, P.S., 2003. Diffusion in biofilms. J. Bacteriol. 185, 1485–1491.
Su, J.F., Zhang, M., Liang, D.H., Wang, J.X., Wang, Z., Li, M., 2019. Performance and microbial community of an immobilized biofilm reactor (IBR) for Mn(II)-based autotrophic and mixotrophic denitrification. Bioresour. Technol. 286, 121407.
Tang, B., Chen, Q.Y., Bin, L.Y., Huang, S.S., Zhang, W.X., Fu, F.L., Li, P., 2018. Insight into the microbial community and its succession of a coupling anaerobic-aerobic biofilm on semi-suspended bio-carriers. Bioresour. Technol. 247, 591–598.
Yang, Z., Peng, X.F., Chen, M.Y., Lee, D.J., Lai, J.Y., 2007. Intra-layer flow in fouling layer on membranes. J. Membr. Sci. 287, 280–286.
Yen, P.S., Chen, L.C., Chien, C.Y., Wu, R.M., Lee, D.J., 2002. Network strength and dewaterability of flocculated activated sludge. Water Res. 36, 539–550.